Progress in Organic Coatings xxx (xxxx) 106609

Contents lists available at ScienceDirect

Progress in Organic Coatings

journal homepage: www.elsevier.com/locate/porgcoat

Oriented immobilization of Pep19-2.5 on antifouling brushes suppresses the development of *Staphylococcus aureus* biofilms

Mariia Vorobii [a, b], Rita Teixeira-Santos [c], Luciana C. Gomes [c], Manuela Garay-Sarmiento [a, b], Anna M. Wagner [a, b], Filipe J. Mergulhão [c, *], Cesar Rodriguez-Emmenegger [a, *]

[a] DWI – Leibniz Institute for Interactive Materials, 52074 Aachen, Germany
[b] Institute of Technical and Macromolecular Chemistry, RWTH Aachen University, 52074 Aachen, Germany
[c] LEPABE – Laboratory for Process Engineering, Environment, Biotechnology and Energy, Faculty of Engineering, University of Porto, Rua Dr. Roberto Frias, 4200-465 Porto, Portugal

ARTICLE INFO

Keywords:
Polymer brushes
Pep. 19-2.5
Antimicrobial coatings
Biofilm
Staphylococci
Strain-promoted alkyne-azide cycloaddition

ABSTRACT

Bacterial colonization of indwelling medical devices poses a danger to the patient and is a tremendous economic burden that costs billions of dollars to the healthcare system. Thus, it is essential to develop an effective mechanism that prevents the attachment of bacteria to the surface in combination with bactericidal strategies to kill them in direct contact. In this work, we combine the repellent/antifouling properties of polymer brushes with the antimicrobial activity of the synthetic peptide Pep19-2.5 and test its efficacy to inhibit *Staphylococcus aureus* biofilm formation. To tackle this, we utilized hierarchical polymer brushes, where the bottom block provides an effective barrier against adhesion while the top block provides functional groups for the immobilization of active molecules. Further, these polymer brushes were decorated with dibenzocyclooctine (DBCO)-functionalized Pep192.5 using strain-promoted alkyne-azide cycloaddition (SPAAC). This click chemistry proceeds very fast and does not require any catalyst, which is crucial for biomedical applications. The obtained coating was not only able to decrease the number of freely planktonic bacteria in the surrounding media (by 52.5%) but also inhibit the development of *S. aureus* biofilm by reducing the number of total, viable, and viable but nonculturable (VBNC) cells (up to 58%, 66%, and 70%, respectively) and reduced the biovolume and thickness. Conversely, this coating does not exert any cytotoxic effect on Normal Human Dermal Fibroblasts (NHDF) cells. Thus, the combination of hierarchical polymer brushes with Pep19-2.5 is a promising approach to fight medical biofilms without affecting surrounding tissues.

1. Introduction

A great number of hospital-acquired infections are associated with bacterial colonization of medical devices and implants [1,2]. In particular, biofilm formation on indwelling medical devices not only causes significant danger to the patients' health and quality of life but also imposes a huge economic burden [3]. For example, catheter-associated urinary tract infections represent 98% of all urinary tract infections, and the total cost of medical bills related to them was estimated to be $36 billion in the US alone [4]. Likewise, prosthetic implants are highly susceptible to bacterial adhesion and the risk of infection after their fixation can reach up to 16% [5]. Implant-associated infection can result in chronic inflammation, malfunction, and may require revision surgeries. Severe cases lead to systemic dissemination of the pathogen that can develop into bacteremia or sepsis [6,7].

Bacterial adhesion starts with the formation of a conditioning film as a result of unspecific protein adsorption called fouling [3]. Fouling inevitably occurs upon contact of foreign material with biological media to reduce the interfacial energy with the material. Upon adhesion, bacteria change their phenotype from freely swimming (planktonic) to sessile and start biofilm formation [8]. Biofilms are complex communities of microorganisms usually associated with a surface and surrounded by a self-produced matrix of extracellular polymeric substance (EPS) [9,10]. The EPS matrix protects bacteria from hostile environments and makes them 10 to 1000 times more resistant to host defense mechanisms, antibiotics, and other antimicrobials in comparison to their planktonic form [11,12]. Moreover, biofilms often contain cells that are viable but non-culturable (VBNC) [13]. These cells are characterized by their inability to form colonies on regular culture media, very low metabolic activity, and higher resistance to chemical and physical

* Corresponding authors.
E-mail addresses: filipem@fe.up.pt (F.J. Mergulhão), rodriguez@dwi.rwth-aachen.de (C. Rodriguez-Emmenegger).

https://doi.org/10.1016/j.porgcoat.2021.106609
Received 23 July 2021; Received in revised form 6 November 2021; Accepted 8 November 2021
0300-9440/

factors in comparison to the culturable cells [13]. Furthermore, VBNC cells can resuscitate and regain their ability to multiply and cause infection when optimal conditions are restored [14]. In general, VBNC cells are resistant to conventional antimicrobial treatments, even after the administration of higher doses of drugs [10]. Therefore, a safer strategy is to prevent the adhesion of bacteria before they can form a more resistant biofilm or become VBNC.

There are two main coating strategies to prevent the bacterial colonization of biomaterials surfaces. The first strategy, antifouling, is based on preventing bacteria attachment by introducing a physical barrier to adhesion [15–17]. The second strategy, bactericidal, is based on killing the microorganism either by the release of a chemical agent or by direct contact with the adhered bacteria [18,19]. The antifouling coatings mainly aim at preventing the formation of a conditioning film induced by protein fouling. In medical devices, only scarce examples based on hydrophilization exist. However, several approaches have been developed in the labs, including self-assembled monolayers (SAMs) [20–22], hydrophilic polymers (e.g. polyethylene glycol, PEG) [23,24], or superhydrophobic materials [25–27]. Usually, these coatings were capable of preventing adsorption from a model solution of a single protein but have limited barrier properties in contact with more complex biological media [28,29]. A more recent strategy is based on graft copolymers in which the adsorption is mediated by physical interactions between the backbone and the substrate. That drives the segregation of the hydrophilic graft away from the surface to generate a brush-like interface. This approach was pioneered by Spencer and Textor and, more recently, by Zuilhof and has resulted in improved repellency compared to other hydrophilic coatings [30–33]. To date, only hydrophilic polymer brushes prepared by the grafting-from approach provide effective antifouling properties [28,34] and reduce forces needed to detach bacteria from the surface by up to 99% in comparison to the bare material [16]. Moreover, polymer brushes based composed of poly[*N*-(2-hydroxypropyl) methacrylamide] (poly(HPMA) showed excellent resistance to protein fouling even after 2 years of storage in buffer [35]. Although antifouling coatings demonstrate excellent protection for short-term contact, prolonged contact with bacteria usually results in the impairment of the surface and colonization [36].

In the case of purely bactericidal coatings, several strategies have been introduced, including silver nanoparticles [37,38], antibiotics [39,40], antimicrobial peptides [41–43], and polycations [44,45]. These strategies are effective at killing pathogenic microorganisms. However, the debris of dead bacteria may accumulate on the surface upon killing, forming a conditioning film that blocks access to the antimicrobial agent, activates the immune response, and creates new anchoring points for bacteria to adhere [3,46,47]. Some bactericidal coatings have limited applicability due to their toxic effect not only on bacterial cells but also on the host [48,49]. Furthermore, only a limited amount of antimicrobials can be introduced in the coating, which can be exhausted before all bacteria have been killed with the concomitant risk to generate the emergence of new drug-resistant strains [50]. Thus, to have an effective performance of the coatings, it is important to combine antifouling properties with a killing mechanism. To date, several reports addressed the combination of repellency and antimicrobial activities [51–54]. However, the bactericidal properties of those coating were tested for a short period (a few hours) in water or buffer. While these conditions serve as a first evaluation, they do not consider the inevitable fouling from protein and the concomitant impairment of the functions of the coating. As result, reported coatings might perform differently in contact with more challenging media over a prolonged period of time. To successfully develop coatings that simultaneously kill and prevent the adhesion of debris, it is crucial to minimize fouling and select suitable antimicrobials and effective methods for their ligation.

In this work, we combined the best antifouling coating with an active killing mechanism to create a synergistic effect against bacterial adhesion. The previous report demonstrates that activation of functional groups alongside the polymer chain and further immobilization of active molecules leads to irreversible reduction of resistance to protein adsorption [55]. To overcome this, we utilized hierarchical polymer brushes reported earlier, which consist of an antifouling bottom block and a functional top block [56–58]. Such architecture allows the introduction of active molecules to the structure without affecting the antifouling properties of the brush. The antifouling block needs to be thick enough to create an effective barrier to adsorption, while the functional block needs to be adjusted to accumulate enough active molecules and do not affect the repellency of the bottom block [59]. For our purpose, the top block was functionalized with azides groups to participate in strain-promoted alkyne-azide cycloaddition (SPAAC) [60]. The benefits of this click chemistry are the absence of catalyst, rapid functionalization that occurs in water and at room temperature, and the inability of azide groups to react nonspecifically with biological molecules. All this provides fast and easy-oriented immobilization of the targeted molecule and is especially important for biomedical applications. To date, this brush architecture was not explored for the preparation of antimicrobial coatings and was mainly used for preparation of biosensors and platform for selective cell capture.

Further, we introduced killing properties to these brushes. The effective killing mechanism needs to be long-lasting and not induce the emergence of resistant strains. One of the most promising candidates is the synthetic antimicrobial peptide Pep19-2.5. The structure of the peptide was inspired by the *Limulus* anti-lipopolysaccharide (LPS) factor and has been optimized by regulating the amount of hydrophobic and positively charged amino acids as well as the length of the peptide [61]. Importantly, this peptide has a wide spectrum of action associated with high affinity not only to the LPS factor of Gram-negative bacteria but also to lipoprotein (LP) of Gram-positive ones [62]. Moreover, recent pioneering studies had shown that Pep19-2.5 reduced bacterial adhesion and biofilm formation of titanium samples from both *Staphylococcus aureus*, *Streptococcus oralis*, *Pseudomonas aeruginosa*, and *Aggregatibacter actinomycetemcomitans* [63]. Furthermore, it demonstrates very low cytotoxicity and can reduce the level of interleukin-6 (IL-6) and tumor necrosis factor-alpha (TNF-α) [64] as well as to attenuate cardiomyopathy in the septic heart [65,66]. Lately, it has been reported that this peptide also inhibits activation of the intrinsic coagulation pathway by significantly reducing the activity of Factor XI [67]. Recently, the high binding affinity of Pep19-2.5 towards Gram-positive and Gram-negative bacteria was explored for capturing bacteria in liquid samples [68]. For this, the peptide was immobilized on the surface of carboxylated magnetic beads by carbodiimide crosslinking. However, the bactericidal activity of peptide Pep19-2.5 upon immobilization was not explored.

We demonstrate that the combination of Pep19-2.5 with polymer brushes was able to reduce the number of planktonic cells in the vicinity of the surface, as well as suppressed *Staphylococcus aureus* biofilm formation by targeting not only culturable but also showing an effect on VBNC cells.

2. Materials and methods

2.1. Materials

Dibenzocyclooctyne (DBCO) functionalized peptide Pep19-2.5 (DBCO-Pep19-2.5), DBCO-$(PEG3)_2$-GCKKYRRFRWKFKGKFWFWG, was synthesized by Biomers.net GmbH. Oligo(ethylene glycol) methyl ether methacrylate (MeOEGMA, M_n = 300 g mol^{-1}), glycidyl methacrylate (≥97.0%, GMA), CuBr (99.999% trace metals basis), $CuBr_2$ (99.999% trace metals basis), 2,2′-bipyridyl (≥99% BiPy), sodium azide (≥99%, ultra-dry, NaN_3) were purchased from Sigma-Aldrich, Germany. Extra dry over Molecular Sieve toluene (99.85%), dimethylformamide (99.8%, DMF), and *N*,*N*-dichloromethane (99.9%, CH_2Cl_2) were purchased from Acros Organic, Germany. Methanol (MeOH), ethanol

(EtOH), acetone, toluene were purchased from VWR Chemicals, Germany. Aluminum oxide 90 basic was purchased from Carl Roth, Germany. Milli-Q water was obtained using Elga™ US filter Purelab Plus UF purification system (PL5113 02), United Kingdom.

11-(Trichlorosilyl)undecyl 2-bromo-2-methylpropanoate [16,69] and ω-mercaptoundecyl bromoisobutyrate [70] were synthesized according to the procedures from the literature.

For the details about ellipsometry, AFM, XPS, and SPR please refer to Supporting Information.

2.2. Immobilization of initiator

Round glass slides 12 mm in diameter were rinsed twice with absolute EtOH and Milli-Q water and blow-dried in an N_2 stream. All samples were activated with oxygen plasma for 20 min (O_2 flow 40 mL min^{-1}, 200 W). Subsequently, the slides were immersed in a freshly prepared 1 mg mL^{-1} solution of 11-(trichlorosilyl)undecyl 2-bromo-2-methylpropanoate initiator in dry toluene. The immobilization was carried out for 3 h in a dry environment to form self-assembled monolayers (SAM) of the initiator. After initiation, samples were rinsed with toluene, acetone, absolute EtOH, and Milli-Q water and dried in an N_2 stream.

2.3. Grafting of polymer brushes

The hierarchical polymer brushes were synthesized according to the procedure described previously [57]. Short description of the procedure:

1) *Antifouling block:* 25 mL of MeOH was deoxygenated by bubbling N_2 for 1 h. Then, 18 mL of deoxygenated MeOH was transferred to a previously degassed flask containing BiPy (556.9 mg, 3.6 mmol), $CuBr_2$ (60.3 mg, 270 μmol), and CuBr (193.8 mg, 1351 μmol) under N_2 atmosphere and stirred till complete dissolution. Simultaneously, MeOEGMA (20.5 g, 68.3 mmol) was dissolved in 18 mL Milli-Q water and degassed by bubbling N_2 for 1 h. Both solutions were mixed and transferred under N_2 protection to a previously degassed reactor containing substrates with SAM of the initiator. After 20 min at 30 °C, the polymerization was stopped by adding Milli-Q water. The substrates were rinsed twice with EtOH and Milli-Q water and dried with N_2.
2) *Azide-functional block:* The inhibitor from the GMA monomer was removed by passing through the basic alumina column. Subsequently, GMA (20.9 g, 147 mmol), BiPy (572.6 mg, 3.7 mmol) $CuBr_2$ (65.7 mg, 294 μmol), and dry DMF (30 mL) were placed in a round-bottom flask and deoxygenated by bubbling N_2 for 1 h. Then, CuBr (210.4 mg, 1.5 mmol) was added under N_2. The mixture was stirred until the full dissolution of the salt and transferred to the reactor containing substrates with the antifouling block, (poly(MeOEGMA). The polymerization was carried out for 4 h at 30 °C. The substrates were rinsed twice with dry DMF and dry $CH_2Cl_2$and dried with N_2.

Afterward, the GMA block was functionalized with azide groups by immersing samples in a 3.4 mg mL^{-1} solution of NaN_3 in dry DMF for 24 h at 60 °C. The samples were rinsed with DMF, EtOH, and Milli-Q water and dried with N_2.

SPR sensor chips were prepared by an analogous procedure but using ω-mercaptoundecyl bromoisobutyrate as initiator. The SAM of the initiator was prepared by immersing a clean SPR chip in 0.6 μL mL^{-1} ethanol solution of the initiator and letting it react for 24 h at room temperature in the dark.

2.4. Immobilization of Pep. 19-2.5

Before immobilization of peptide, polymer brushes were placed in water and let swell overnight. Then, a solution of Pep.19-2.5 in phosphate-buffered saline (PBS) with a concentration of 100 μg mL^{-1} was prepared. Samples were immersed in peptide solution and incubated overnight at room temperature. Then, samples were washed with PBS buffer and stored in it till further use.

2.5. Bacteria and growth conditions

An overnight culture was prepared as described by Moreira et al. [71]. Briefly, 500 μL of bacterial cells stored in 20% (v/v) glycerol at −80 °C was added to a total volume of 200 mL LB medium (Lennox, Sigma-Aldrich, Saint Louis, MO, USA) and incubated overnight at 37 °C with a constant orbital agitation of 160 rpm. Subsequently, cells were harvested by centrifugation at 3202*g*, 25 °C for 10 min (Eppendorf Centrifuge 5810R, Hamburg, Germany), and washed once in 0.85% (v/v) NaCl (VWR International, Carnaxide, Portugal). A cell suspension was prepared in saline solution, adjusted to an optical density ($OD_{600\ nm}$) of 0.1, and then, serially 6-fold diluted to obtain a cell concentration ≤ 10^2 cells mL^{-1}.

2.6. Antimicrobial activity of peptide DBCO-Pep19-2.5

To determine the antimicrobial activity of the free peptide, a solution of DBCO-Pep19-2.5 was prepared in PBS at a concentration of 100 μg mL^{-1}. Since the synthesized surfaces contained 339 ng peptide (as detected by SPR) and were further inoculated with 3 mL bacterial suspension for biofilm assays, the DBCO-Pep19-2.5 solution was diluted in LB medium to obtain a concentration of 236.7 ng mL^{-1}. Subsequently, 1.5 mL of peptide solution was added to 1.5 mL of *S. aureus* suspension with cell concentration ≤ 10^2 cells mL^{-1} and incubated at 37 °C, for 24 h without agitation. Then, bacterial suspension was properly diluted and spread on plate count agar (PCA, Oxoid, UK), and incubated overnight at 37 °C. The culturability of cells exposed to peptide was determined by CFU counting and compared with control (cells not exposed to DBCO-Pep19-2.5). Antimicrobial experiments were performed in three independent assays, each one with two technical replicates.

2.7. S. aureus biofilm formation

Biofilm formation assays were performed in 12-well microtiter plates (VWR International, Carnaxide, Portugal) under static conditions. Sterilized surfaces, including the glass, MeOEGMA-N_3, and MeOEGMA-Pep19-2.5 surfaces, were placed on the microplate wells and inoculated with 3 mL of a bacterial suspension at a concentration ≤ 10^2 cells mL^{-1}. Besides, 3 mL of LB medium was added to the wells containing sterilized surfaces to control their sterility throughout the experiments. Plates were incubated at 37 °C for 24 h. Biofilm formation experiments were performed in three independent assays, each one with three technical replicates.

2.8. Bacterial cells quantification

After 24 h biofilm formation on glass, brush, and MeOEGMA-Pep19–2.5 surfaces, planktonic and biofilm cells were analyzed. Firstly, the supernatant was collected from microplate wells and was properly diluted and spread on PCA for CFU enumeration. Subsequently, biofilm cell suspensions were obtained by dipping each surface in 2 mL 0.85% (v/v) NaCl and vortexing for 3 min. Biofilm cell culturability was assessed by spreading the biofilm suspension on PCA followed by CFU counting (CFU cm^{-2}). In turn, biofilm viability was evaluated by staining the biofilm suspension with the Live/Dead® BacLight™ Bacterial

Viability kit (Invitrogen Life Technologies, Alfagene, Portugal) as previously described [72], and analyzing in an epifluorescence microscope (Leica DM LB2, Germany). A minimum of twenty fields of view was analyzed for each stained sample using the ImageJ software (version 1.52p, National Institutes of Health, EUA) and the number of total and viable cells was counted. In addition, the number of VBNC cells was determined by subtracting the number of culturable cells from that of viable cells [13]. The number of total, viable and VBNC cells were expressed as cells cm^{-2}.

2.9. Assessment of biofilm structure by confocal laser scanning microscopy (CLSM)

CSLM was performed as described before [14]. Briefly, 24-hour biofilms formed on the glass, brush, and MeOEGMA-Pep19-2.5 surfaces were counterstained in green with 6 μM SYTO® 9 (Thermo Fisher Scientific, USA) and observed using a 10× dry objective (Leica HC PLAN APO CS) in an inverted microscope Leica DMI6000-CS (Leica Microsystems, Germany) with a 488-nm argon laser. Images were acquired with 512 × 512 pixels and a *z*-step of 1 μm in a minimum of six different regions of each analyzed surface.

Three-dimensional (3D) projections of biofilm structures were reconstructed using the "Easy 3D" tool of IMARIS 9.1 software (Bitplane, Switzerland) directly from the CLSM acquisitions. The plug-in COMSTAT2 associated with the ImageJ software was used to determine the biovolume ($\mu m^3\ \mu m^{-2}$) and the biofilm thickness (μm) [73].

2.10. Statistical analysis

Descriptive statistics were used to calculate the mean and standard deviations for the number of culturable (Fig. 4), total, viable and VBNC cells (Fig. 6), and biovolume and biofilm thickness (Fig. 5B). Differences between the number of cells obtained for glass, brush, and MeOEGMA-Pep19-2.5 surfaces (Figs. 4 and 6) were evaluated using unpaired *t*-tests or Mann-Whitney tests according to the normality of the variables' distributions. Quantitative parameters obtained from confocal microscopy (Fig. 5B) were compared using a one-way analysis of variance (ANOVA). All tests were performed with a confidence level of 95% (p-values <0.05). Data analysis was performed using the IBM SPSS Statistics version 24.0 for Windows (IBM SPSS, Inc., Chicago, IL, USA).

3. Results and discussion

3.1. Grafting of polymer brushes and characterization

Surfaces that combine both antifouling and antimicrobial properties are in high demand for biomedical applications. To combine antifouling properties with functionality, hierarchical polymer brushes were prepared using surface-initiated atom transfer radical polymerization (SI-ATRP). The first block consists of poly(oligo(ethylene glycol) methyl ether methacrylate) (poly(MeOEGMA)) grafted from a self-assembled monolayer (SAM) of the silane initiator. The bottom block was chain-extended with poly(glycidyl methacrylate) (poly(GMA)). Finally, the epoxide group of poly(GMA) block was functionalized with azide groups forming poly(3-azido-2-hydroxypropyl methacrylate functional block (Scheme 1A).

Ellipsometry, X-ray photoelectron spectroscopy (XPS), and atomic force microscopy (AFM) were utilized to confirm the successful preparation of hierarchical polymer brushes. Si wafers were utilized as model substrates to determine the dry ellipsometric thickness of each layer. The analysis shows that the initial thickness of the initiator layer was about 1 nm. Topographic AFM images reveal a homogeneous layer, absence of pinholes, and low roughness $R_q = 0.57 \pm 0.04$ nm (Fig. 1A). The chemical composition of SAM was confirmed by XPS. The XPS spectrum of the C1s region shows the predominant band at 285.0 eV that corresponds to C—C and C—H components of the long alkyl backbone. Moreover, further deconvolution of the envelope reveals C—O and O═C—O components of the ester group resolved at 286.7 and 289.0 eV, respectively. All peaks resemble the chemical structure

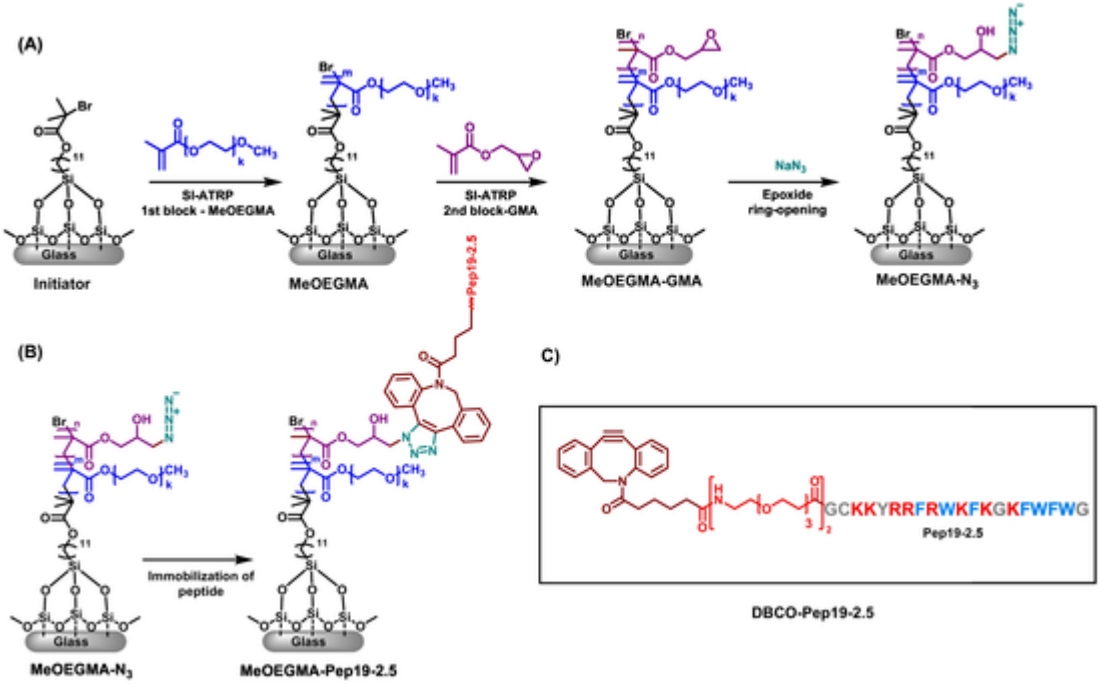

Scheme 1. The synthetic route was followed to prepare polymer brushes functionalized with DBCO-Pep19-2.5. (A) Grafting of polymer brushes. (B) SPAAC immobilization of DBCO-Pep19-2.5 and (C) Chemical structure of DBCO-Pep192.5 and its amino acid sequence. Amino acids: G, glycine; C, cysteine; K, lysine Y, tyrosine; R, arginine; F, phenylalanine; W, tryptophan. The colors illustrate characteristics of amino acids: red - cationic, positively charged, blue - hydrophobic, and grey - polar. For the complete chemical structure of DBCO-Pep19-2.5 refer to Fig. S1.

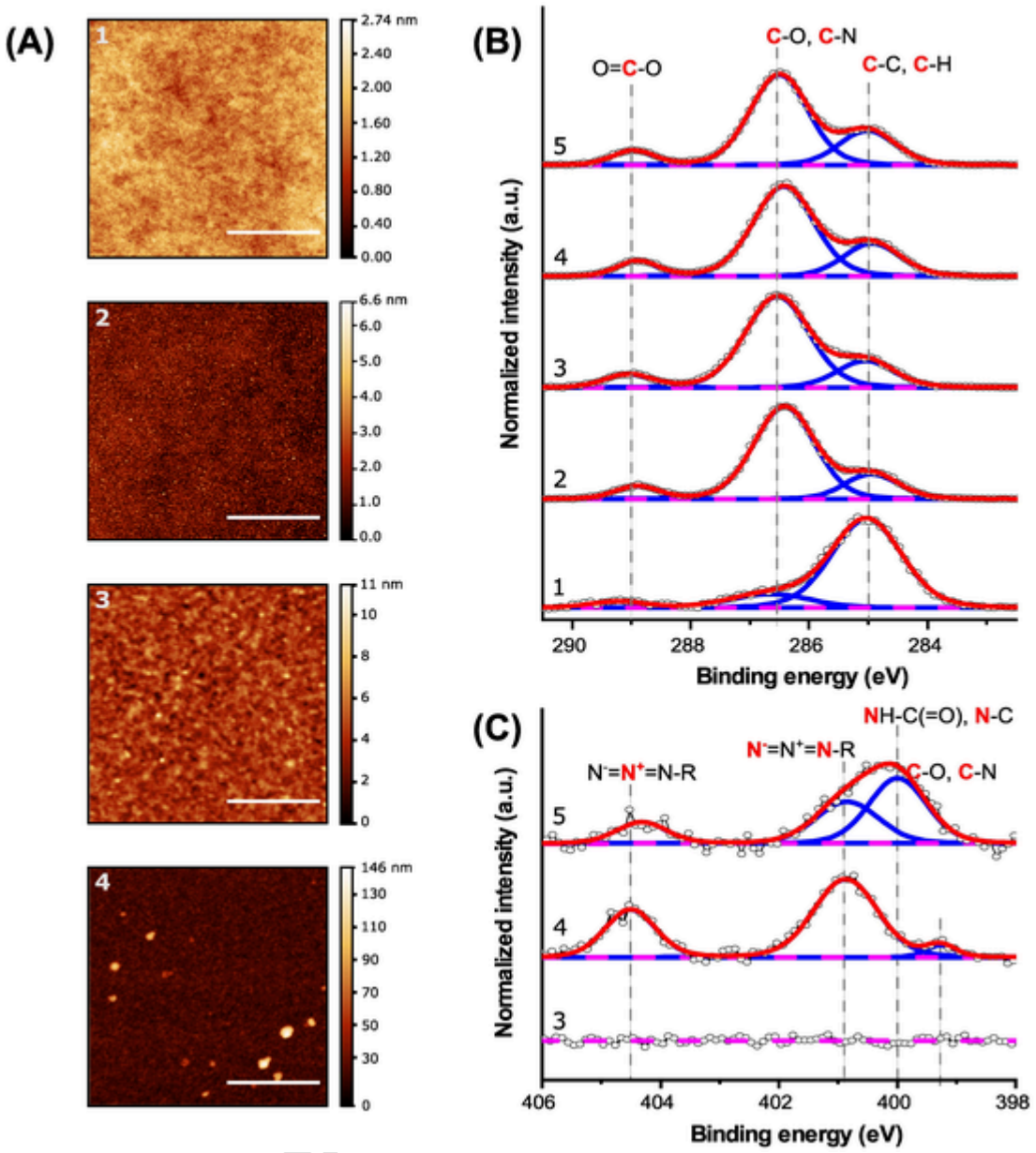

Fig. 1. (A) AFM topography of 1) glass, 2) SAM of initiator, 3) MeOEGMA-N_3, and 4) MeOEGMA-Pep19-2.5 measured by tapping mode in air. The scale bar is 2 μm. (B) High-resolution XPS spectra of C1s region of 1) Initiator, 2) MeOEGMA, 3) MeOEGMA-GMA, 4) MeOEGMA-N_3, and 5) MeOEGMA-Pep19-2.5. (C) High-resolution XPS spectra of N1s region of 3) MeOEGMA-GMA, 4) MeOEGMA-N_3, and MeOEGMA-Pep19-2.5.

of the initiator, which is composed of a long alkyl chain and a single ester group.

The grafting of the diblock led to an increase in thickness and a change in chemical composition. The thickness increased to 29 nm after the preparation of poly(MeOEGMA). Further, a 5 nm poly(GMA) block was grafted. This thickness is optimal to have a sufficient amount of Pep19-2.5 while not affecting the antifouling properties of MeOEGMA. The glycidyl groups were utilized to introduce azide groups by reacting the brushes with sodium azide. Functionalization of MeOEGMA-GMA with sodium azide did not change the thickness of the layer. The topography of the MeOEGMA-N_3 functionalization with azide was assessed by AFM. Fig. 1A-3 shows a homogeneous surface, without pinholes and roughness of R_q = 0.91 ± 0.12 nm. The XPS spectrum of the C1s region shows a predominant peak at 286.5 eV that corresponds to the C—O components of the poly(MeOEGMA) side chain, while a band at 289.0 eV can be assigned to the ester group O═C—O present in the methacrylate backbone. The structure of poly (MeOEGMA) was further confirmed by analyzing the area ratio between the (C—O):(C—C, C—H). The value of 4.08 indicates that the C—O component from the side chain is predominant of the C—C and C—H groups that are present only in the polymer backbone, which is in accordance with the structure. The C1s XPS spectrum of diblock, MeOEGMA-GMA, only slightly differs from the bottom block of MeOEGMA. The area ratio between the (C—O):(C—C, C—H) bonds of the diblock slightly decreased to 3.84, which is associated with an increased number of C—C and C—H groups associated with side chains of poly(GMA) block. The AFM topography images of both MeOEGMA and MeOEGMA-GMA show a homogeneous surface with low roughness R_q = 0.88 ± 0.18 nm and R_q = 0.81 ± 0.29 nm respectively (Fig. S2). Further, glycidyl groups were reacted with sodium azide resulted in ring-opening and formation of functional MeOEGMA-N_3 surface. The successful functionalization was evidenced in the N1s region of the XPS spectrum (Fig. 1C-4). The bands at 400.9 and 404.5 eV are characteristic of the N atom in the organic azide group. The small peak at 399.3 eV

is the result of the degradation of the organic azide group under X-ray irradiation. Moreover, no signal in the N1s spectrum was observed for MeOEGMA-GMA (Fig. 1C-3).

3.2. Immobilization of DBCO-Pep19-2.5

Non-oriented immobilization of peptides and proteins often decreases their biological activity [74]. This is further aggravated if the immobilization is carried out by non-specific amidation of lysine residues which may be part of the biologically active center of the protein and especially crucial in the case of small peptides. In this work, we utilized a specially designed dibenzocyclooctine (DBCO) functionalized Pep19-2.5 (DBCO-Pep19-2.5). The DBCO group with (tri(ethylene glycol)) spacer was attached to the N-terminus of peptide (Scheme 1C). Upon contact with an azide group, DBCO undergoes catalyst-free SPAAC reaction and covalently binds the peptide to the surface through the N-terminus, exposing the C-terminus to the outside (Scheme 1B). This type of functionalization does not involve any side groups of the Pep19-2.5 sequence.

The immobilization of DBCO-Pep19-2.5 was quantified by surface plasmon resonance (SPR). For this, hierarchical polymer brushes were grafted from a SAM of ω-mercaptoundecyl bromoisobutyrate on gold-coated SPR sensors. During the measurements, the brushes were equilibrated in phosphate-buffered saline (PBS) buffer. After a steady baseline was reached, PBS buffer was replaced with 100 μg mL^{-1} solution of DBCO-Pep19-2.5 and a sensogram was recorded at 10 μL min^{-1} for 80 min (Fig. 2A) followed by washing with the running buffer. The surface coverage was determined to be 299.62 ± 2.86 ng cm^{-2}. Fig. 1A-4 shows the topology of the polymer brush after functionalization with Pep19-2.5 as depicted by the AFM. In general, the surface remained homogeneous with a slight increase of roughness (R_q = 4.09 ± 0.57 nm) in comparison to the bare brush. To further prove the successful immobilization of the peptide, an XPS measurement was performed (Fig. 1C-5). The high-resolution N1s spectra after functionalization with Pep19-2.5 shows the predominant peak at 400 eV of amide NH—(C═O) that was not present before and is characteristic for peptides and proteins (Fig. 1C).

3.3. Antifouling properties

We assessed whether the immobilization of DBCO-Pep19-2.5 onto MeOEGMA-N_3 brushes impaired their resistance to protein adsorption using SPR. The fouling studies were performed in two different media: 1) Luria–Bertani broth (LB) as media used in bacterial studies (Sections 3.5 and 3.6) and 2) undiluted blood plasma (BP) as one of the most challenging biological media. Data was compared to bare gold and MeOEGMA-N_3 and summarized in Fig. 2C. The contact of LB and PB with bare gold led to rapid protein adsorption from both tested media. In contrast, MeOEGMA-N_3 was able to reduce the adsorption of proteins from BP by 79.3% and from LB by 84.3%. A similar reduction of protein adsorption from BP (81.3%) and LB medium (86%) was obtained for MeOEGMA-Pep19-2.5 brushes. Thus, the functionalization of MeOEGMA-N_3 with the peptide did not impair their antifouling properties.

3.4. Biocompatibility of MeOEGMA-Pep19-2.5 coating

We assessed the cytocompatibility of the MeOEGMA-Pep19-2.5 coating, by studying the viability (in vitro) of Normal Human Dermal Fibroblasts (NHDF) after direct contact. Tests were performed according to the International Organization for Standardization 109993-5 (ISO109993-5). Coated glass slides were placed on top of a monolayer of NHDF cells and incubated for 24 h at 37 °C in a humidified, 5% CO_2 atmosphere. Then, the viability of cells was visualized using LIVE/DEAD® staining. Fluorescence micrographs were acquired from the cell monolayer directly in contact with the coating (region I, in the scheme in Fig. 3A and 3B-I). All the tested samples showed a high number of viable cells (green) and single or none dead cells (red). Moreover, there was no significant morphological difference between the cells that were in direct contact with samples (Fig. 3B-I) and cells were next to it in the same well plate (Fig. 3B-II), and even with control samples in which cells were cultivated without contact with any sample (see Fig. S5 and S6).

The cell viability was quantified by the colorimetric MTS assay. Samples were placed similarly as above and after incubation time 24 h MTS test was performed (Table S1). NHDF in direct contact with glass without any modification were taken as 100% reference (Fig. 3C). There was no significant difference in the metabolic activity between the coated samples and the control. The results demonstrate that cell viability was not impaired after direct contact with MeOEGMA-N_3 and MeOGMA-Pep19-2.5 coatings.

3.5. Antimicrobial activity of the free and immobilized DBCO-Pep19-2.5

We studied the antimicrobial activity of immobilized DBCO-Pep19-2.5 against *S. aureus* ATCC 25923. *S. aureus* was selected it is one of the most common microorganisms isolated from implant-associated infections [3,75], and is known to express a high number of surface adhesins that promote attachment [76].

Firstly, we tested the activity of free DBCO-Pep19-2.5 to confirm that after N-terminal functionalization with dibenzocyclooctyne group the peptide still displays a bactericidal effect on the tested *S. aureus* strain (Fig. 4A). Dissolved DBCO-Pep19-2.5 (339 ng) was added to 3 mL of a bacteria suspension with 10^2 CFU mL^{-1} for 24 h. The amount of peptide was the same as the one immobilized on the surface of the substrate utilized in the following studies and was calculated based on

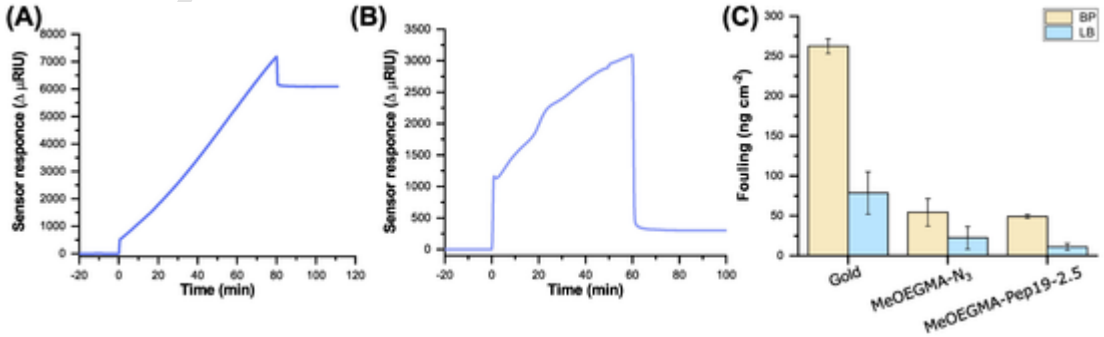

Fig. 2. (A) SPR sensogram showing immobilization of DBCO-Pep19-2.5 on the surface of the polymer brushes. (B) Protein fouling of Luria–Bertani (LB) medium on the surface of MeOEGMA-Pep19-2.5 as detected by SPR. (C) Histogram showing protein fouling of LB media and undiluted blood plasma (BP) on the surface of bare SPR chip (gold), MeOEGMA-N_3, and MeOEGMA-Pep19-2.5. (For interpretation of the references to colour in this figure legend, the reader is referred to the web version of this article.)

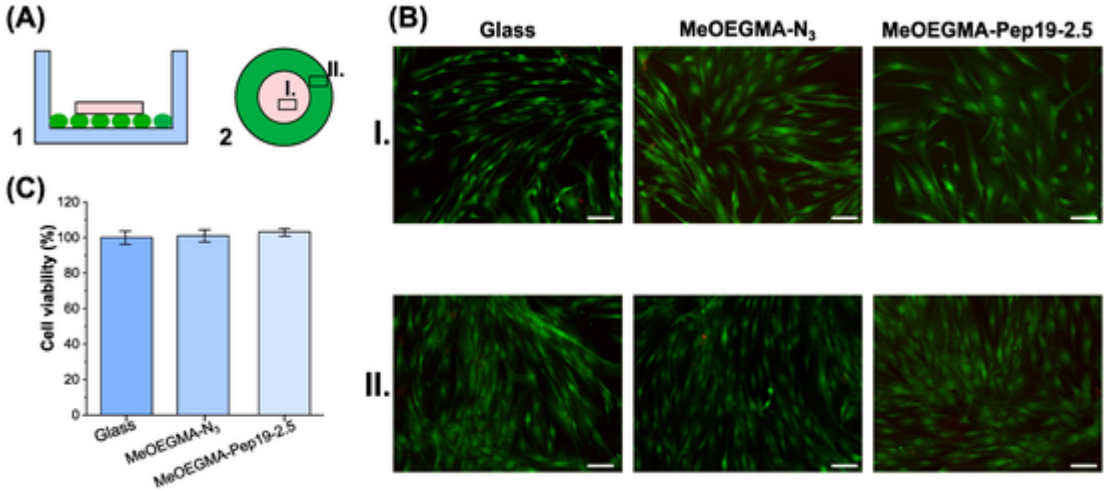

Fig. 3. (A) Scheme of direct contact cytotoxicity assay: 1) incubation of tested samples (pink) with a monolayer of cells (green) and 2) microscopic images were obtained from two locations in the well: (I) in direct contact with the sample, (II) edges without contact. (B) Representative ApoTome fluorescence micrographs of NHDF cells stained with LIVE/DEAD® assay after 24 h incubation with glass, MeOEGMA-N_3, and MeOEGMA-Pep19-2.5. The micrographs were taken in the area of the sample (I) and in the area next to the sample (II). The scale bar is 100 μm. (C) Viability of NHDF cells upon contact with glass, MeOEGMA-N_3, and MeOEGMA-Pep19-2.5. Cell viability was measured by MTS assay. Absorbance was measured at 490 nm and normalized, where the absorbance of the glass sample serves as 100% reference. There was no significant difference for *p*-values <0.05. (For interpretation of the references to colour in this figure legend, the reader is referred to the web version of this article.)

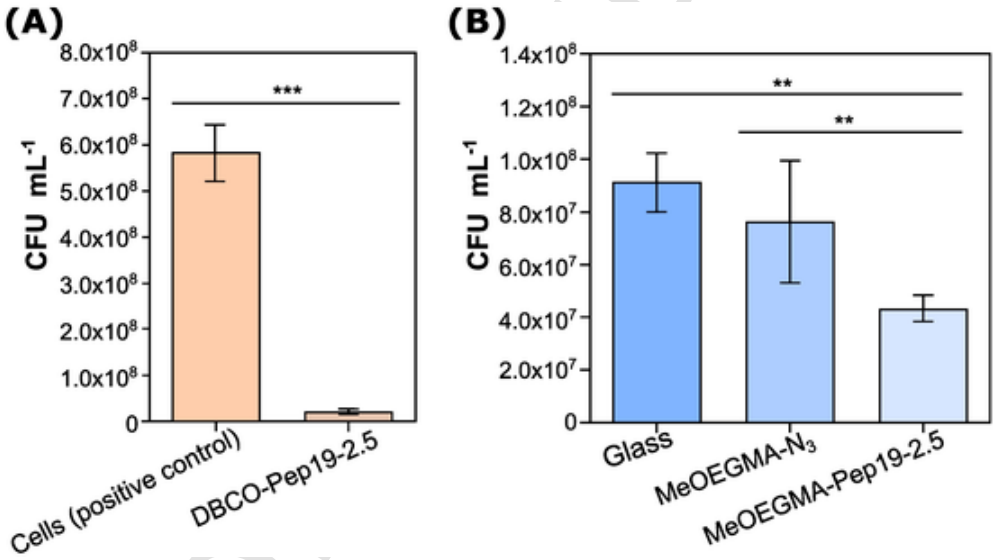

Fig. 4. Colony-forming units counting of supernatant after 24 h incubation of cells with (A) free DBCO-Pep19-2.5 in LB medium and (B) with bare glass, and glass coated with MeOEGMA-N_3 and MeOEGMA-Pep19-2.5. Significant differences were considered for *p*-values <0.05 (*** $p < 0.001$, ** $p < 0.01$).

the surface area of the planar surface used for the antimicrobial test (glass slides, ⌀ 12 mm), and the surface coverage was determined by SPR. The number of culturable bacteria that remained in the supernatant after 24 h incubation with the peptide was reduced by 96.0%, as determined by colony-forming units (CFU) counts. Thus, the tested free peptide displayed antimicrobial activity against *S. aureus* ATCC 25923. The activity of the immobilized peptide (MeOEGMA-Pep19-2.5) was monitored by incubating the substrates with a starting concentration of *S. aureus* $\leq 10^2$ CFU mL^{-1} for 24 h. Bare glass slides and MeOEGMA-N_3 were used as controls. Then, the number of culturable bacteria that remained in the supernatant was determined by CFU counts. The MeOEGMA-Pep19-2.5 coating reduced the number of culturable cells by 52.5% in comparison to the glass surface, while only a minor reduction (16.4%) was observed for the MeOEGMA-N_3 control (Fig. 4B). These results, on the one hand, demonstrate that the peptide could significantly decrease the concentration of bacteria but on the other hand that the activity was lower than with the free peptide. The comparatively lower activity of the immobilized peptide could be caused by a decrease in mobility and concomitant impaired ability of the peptide to bind to *S. aureus*. Another possible cause is that not all bacteria could come in contact with the surface for the bactericidal action to occur. To probe these two scenarios, it was necessary to observe the biofilm formation on the surfaces tested.

3.6. Biofilm formation on MeOEGMA-Pep19-2.5

The effect of the immobilized Pep19-2.5 against *S. aureus* biofilm formation was observed by confocal laser scanning microscopy (CLSM) after staining it with SYTO® 9 (Fig. 5A) [14,77–79]. *S. aureus* formed dense and thick biofilm on glass (control surface). The biofilm was a confluent layer with a thickness of about 90 μm and a biovolume of 33 $\mu m^3 \cdot \mu m^{-2}$ as evidenced in Fig. 5 and Table S2. The addition of poly-

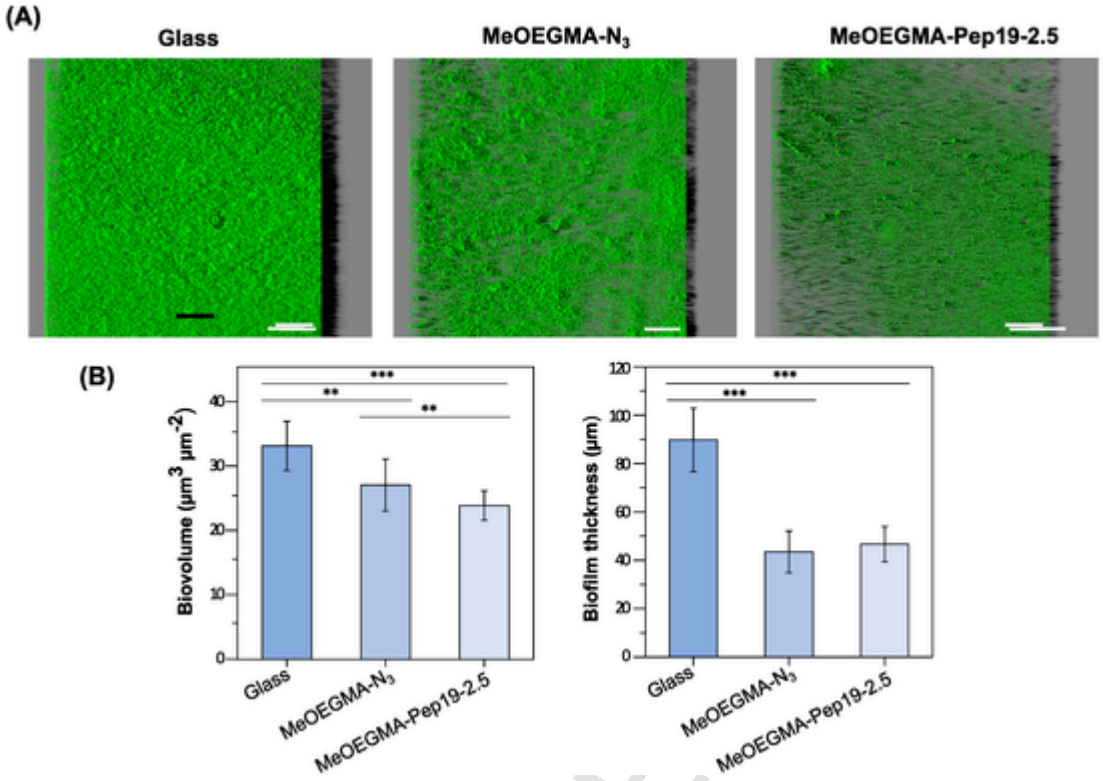

Fig. 5. (A) Representative biofilm structures of *S. aureus* on glass, MeOEGMA-N_3, and MeOEGMA-Pep19-2.5 surfaces. These images were obtained from confocal *z*-stacks using IMARIS software and present an aerial, three-dimensional (3D) view of the biofilms (shadow projection on the right). The scale bar is 200 μm. (B) Biovolume and biofilm thickness values were obtained from the *z*-stacks using the COMSTAT2 tool associated with the ImageJ software. Statistical analysis was performed using one-way analysis of variance (ANOVA) and significant differences were considered for *p*-values <0.05 (*** $p < 0.001$, ** $p < 0.01$, * $p < 0.05$).

mer brushes MeOEGMA-N_3 resulted in a non-confluent biofilm with a thickness of 44 μm and biovolume of 27 $\mu m^3 \cdot \mu m^{-2}$. Although biofilms formed on MeOEGMA-N_3 surfaces had about 18.4% and 51.5% less biovolume and thickness, respectively, than those developed on glass ($p < 0.01$ and $p < 0.001$, respectively; Fig. 5B), the typical *S. aureus* biofilm high-density cell clusters [80,81] were still detected on the modified glass surface (Fig. 5A). A similar thickness reduction was observed in a previous work of the research group when the antibiofilm potential of poly(MeOEGMA) brush was tested against *E. coli* under flow conditions [82]. The functionalization with Pep19-2.5 afforded a further decrease in biofilm formation, with a biovolume reduction of 24.2% compared to glass. A similar reduction of biofilm biovolume was reported for *S. aureus* biofilm treated with free Pep19-2.5 (without DBCO) [63]. Moreover, the architecture of the biofilm on MeOEGMA-Pep19-2.5 is drastically different than the ones observed on glass and MeOEGMA-N_3. While bacteria formed confluent films on the control surface, scattered aggregates below the percolation threshold were observed on those surfaces decorated by Pep19-2.5. Thus, not only did the peptide suppress the biofilm formation but drastically impaired its ability to form continuous films.

Further, the cellular composition of biofilms formed on the glass, MeOEGMA-N_3, and MeOEGMA-Pep19-2.5 was evaluated by counting total, viable, and VBNC cells (Fig. 6). Firstly, the biofilm was detached from the substrate. The number of total and viable cells was determined by epifluorescence microscopy using the Live/Dead staining, where the green-fluorescent dye (SYTO® 9) penetrates all cells, while red-fluorescent dye (propidium iodide) penetrates only cells with impaired membranes. The number of VBNCs was calculated as the difference between the viable cells and the culturable cells (determined by CFU counting).

The analysis of total cells indicates that biofilms formed on the MeOEGMA-N_3 surfaces exhibited 44.4% fewer *S. aureus* cells than glass

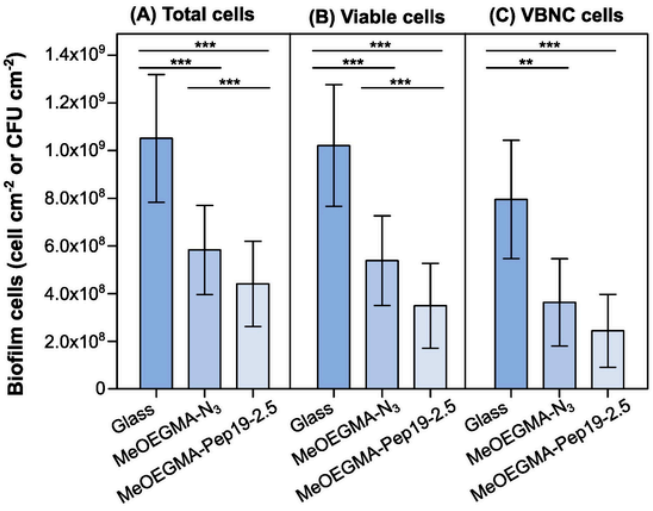

Fig. 6. The number of (A) total, (B) viable, and (C) viable but nonculturable (VBNC) cells after 24 h of biofilm development on glass, MeOEGMA-N_3, and MeOEGMA-Pep19-2.5 surfaces. Inferential statistics were performed using unpaired *t*-tests or Mann–Whitney tests according to the normality of the variables' distributions. Significant differences were considered for *p*-values <0.05 (*** $p < 0.001$, ** $p < 0.01$, * $p < 0.05$).

($p < 0.001$). The reduction of the number of total bacteria adhered to the MeOEGMA-N_3 brush is in line with previous studies showing that the MeOEGMA brushes could reduce the work of adhesion of a bacterium (*Y. pseudotuberculosis*, a Gram-negative bacterium) to values between 2% and 10% of the values observed on glass. [16] Additionally, Alves et al. [82] demonstrated that *Escherichia coli* cells adhered 43.0% less to a poly(MeOEGMA) brush than to PDMS after 24 h of biofilm de-

velopment under urinary flow conditions. Furthermore, the antiadhesive effect of MeOEGMA-N_3 was improved by the immobilization of DBCO-Pep19-2.5, exhibiting 58.0% fewer *S. aureus* cells than glass ($p < 0.001$).

Moreover, MeOEGMA-Pep19-2.5 surfaces reduced the viability of bacteria by about 66.0 and 35.0% compared to glass and MeOEGMA-N_3 surfaces, respectively ($p < 0.001$). It is known that Pep19-2.5 displays a high affinity to lipoproteins (in the case of Gram-positive bacteria like *S. aureus*), which facilitates peptide binding and its insertion into the bacterial outer membrane [83,84]. Similar to what happens with most antimicrobial peptides, when the peptide reaches a critical concentration, the bacterial membrane starts to destabilize and permeabilizes, leading to cell death [84]. Interestingly, in the study of Subh et al. [63] the free Pep19-2.5 did not show a significant reduction of viable cells in *S. aureus* biofilm. However, this study was performed with another *S. aureus* strain and utilized different testing conditions.

The MeOEGMA-Pep19-2.5 surface also significantly reduced the number of VBNC cells by 70.0 ($p = 0.001$) and 33.0% ($p = 0.225$) compared to glass and brush surfaces, respectively. The VBNC state is an important survival strategy adopted by many bacteria when exposed to unfavorable environmental conditions [85]. These cells remain viable over long periods, even under continued stress conditions, but lose their culturability in conventional media, thus impairing their detection by traditional plate counting techniques [13,85].

4. Conclusions

We developed a coating that combined repellent properties with a killing mechanism using a combination of hierarchical polymer brushes with Pep19-2.5. For the first time, we studied the antimicrobial activity of this peptide after immobilization to the surface. We demonstrate that N-terminal functionalization of Pep19-2.5 with DBCO before immobilization does not impair its antimicrobial activity against *S aureus*. Although the activity of the immobilized peptide was lower than in the free state, the decoration of MeOEGMA brushes with Pep19-2.5 improved their performance, reduced biofilm formation, and prevented the development of a confluent film. Moreover, it reduced the number of *S. aureus* VBNC cells in the biofilm. Furthermore, we demonstrated that obtained coating did not have any cytotoxic effect on NHDF, proving excellent biocompatibility. These results are promising since, in clinical scenarios, VBNCs can become resistant to antimicrobial drugs and reinitiate infection when appropriate conditions are established.

Declaration of competing interest

The authors declare that they have no known competing financial interests or personal relationships that could have appeared to influence the work reported in this paper.

Acknowledgments

The authors thank the support of the Research Association of Forschungskuratorium Textil e.V. supported via AiF (“Arbeitsgemeinschaft Industrielle Forschungsvereinigungen Otto von Guericke e.V.”), research project IGF-No. 19893N within the promotion program of “Industrielle Gemeinschaftsforschung” (IGF) of the Federal Ministry for Economic Affairs and Energy on the basic of a decision by the German Bundestag. The authors also acknowledge the support of H2020-NMBP-TRIND-2018, EVPRO (Development of Extracellular Vesicles loaded hydrogel coatings with immunomodulatory activity for Promoted Regenerative Osseointegration of revision endoprosthesis) grant 814495-2. This work was also partially performed at the Center of Chemical Polymer Technology CPT, which was supported by the EU and the Federal State of North Rhine-Westphalia (grant EFRE 30 00 883 02).

This work was also supported by Base Funding - UIDB/00511/2020 of the Laboratory for Process Engineering, Environment, Biotechnology and Energy - LEPABE - funded by national funds through the FCT/MCTES (PIDDAC), and by the European Union's Horizon 2020 research and innovation programme under grant agreement No 952471. R.T.-S. thanks the receipt of a junior researcher fellowship from the Project PTDC/BII-BIO/29589/2017 - POCI-01-0145-FEDER-029589 - funded by FEDER funds through COMPETE2020 - Programa Operacional Competitividade e Internacionalização (POCI) and by national funds (PIDDAC) through FCT/MCTES. L.C.G. thanks the Portuguese Foundation for Science and Technology (FCT) for the financial support of her work contract through the Scientific Employment Stimulus—Individual Call—[CEECIND/01700/2017].

Appendix A. Supplementary data

Supplementary data to this article can be found online at https://doi.org/10.1016/j.porgcoat.2021.106609.

References

[1] R.O. Darouiche, Treatment of infections associated with surgical implants, N. Engl. J. Med. 350 (2004) 1422–1429, https://doi.org/10.1056/NEJMra035415.
[2] S.S. Magill, J.R. Edwards, W. Bamberg, Z.G. Beldavs, G. Dumyati, M.A. Kainer, R. Lynfield, M. Maloney, L. McAllister-Hollod, J. Nadle, S.M. Ray, D.L. Thompson, L.E. Wilson, S.K. Fridkin, I. Emerging Infections Program Healthcare-Associated, T. Antimicrobial use prevalence survey, multistate point-prevalence survey of health care-associated infections, N. Engl. J. Med. 370 (2014) 1198–1208, https://doi.org/10.1056/NEJMoa1306801.
[3] C.R. Arciola, D. Campoccia, L. Montanaro, Implant infections: adhesion, biofilm formation and immune evasion, Nat. Rev. Microbiol. 16 (2018) 397–409, https://doi.org/10.1038/s41579-018-0019-y.
[4] M. Ramstedt, I.A.C. Ribeiro, H. Bujdakova, F.J.M. Mergulhao, L. Jordao, P. Thomsen, M. Alm, M. Burmolle, T. Vladkova, F. Can, M. Reches, M. Riool, A. Barros, R.L. Reis, E. Meaurio, J. Kikhney, A. Moter, S.A.J. Zaat, J. Sjollema, Evaluating efficacy of antimicrobial and antifouling materials for urinary tract medical devices: challenges and recommendations, Macromol. Biosci. 19 (2019) e1800384, https://doi.org/10.1002/mabi.201800384.
[5] W. Zimmerli, Clinical presentation and treatment of orthopaedic implant-associated infection, J. Intern. Med. 276 (2014) 111–119, https://doi.org/10.1111/joim.12233.
[6] A.G. Gristina, J.W. Costerton, Bacterial adherence to biomaterials and tissue. The significance of its role in clinical sepsis, J. Bone Jt. Surg. 67-A 67–A (1985) 264–273.
[7] G. Donelli, Vascular catheter-related infection and sepsis, Surg. Infect. 7 (Suppl. 2) (2006) S25–S27, https://doi.org/10.1089/sur.2006.7.s2-25.
[8] T.R. Garrett, M. Bhakoo, Z. Zhang, Bacterial adhesion and biofilms on surfaces, Prog. Nat. Sci. 18 (2008) 1049–1056, https://doi.org/10.1016/j.pnsc.2008.04.001.
[9] L. Hall-Stoodley, J.W. Costerton, P. Stoodley, Bacterial biofilms: from the natural environment to infectious diseases, Nat. Rev. Microbiol. 2 (2004) 95–108, https://doi.org/10.1038/nrmicro821.
[10] H.C. Flemming, J. Wingender, The biofilm matrix, Nat. Rev. Microbiol. 8 (2010) 623–633, https://doi.org/10.1038/nrmicro2415.
[11] B.D. Hoyle, J.W. Costerton, Bacterial resistance to antibiotics: the role of biofilms, Prog. Drug Res. 37 (1991) 91–105, https://doi.org/10.1007/978-3-0348-7139-6_2.
[12] H. Ceri, M.E. Olson, C. Stremick, R.R. Read, D. Morck, A. Buret, The Calgary biofilm device: new technology for rapid determination of antibiotic susceptibilities of bacterial biofilms, J. Clin. Microbiol. 37 (1999) 1771–1776, https://doi.org/10.1128/JCM.37.6.1771-1776.1999.
[13] L. Li, N. Mendis, H. Trigui, J.D. Oliver, S.P. Faucher, The importance of the viable but non-culturable state in human bacterial pathogens, Front. Microbiol. 5 (2014) 258, https://doi.org/10.3389/fmicb.2014.00258.
[14] P. Alves, L.C. Gomes, M. Vorobii, C. Rodriguez-Emmenegger, F.J. Mergulhao, The potential advantages of using a poly(HPMA) brush in urinary catheters: effects on biofilm cells and architecture, Colloids Surf. B: Biointerfaces 191 (2020) 110976, https://doi.org/10.1016/j.colsurfb.2020.110976.
[15] R. Zhang, Y. Liu, M. He, Y. Su, X. Zhao, M. Elimelech, Z. Jiang, Antifouling membranes for sustainable water purification: strategies and mechanisms, Chem. Soc. Rev. 45 (2016) 5888–5924, https://doi.org/10.1039/c5cs00579e.
[16] C. Rodriguez-Emmenegger, S. Janel, A. de los Santos Pereira, M. Bruns, F. Lafont, Quantifying bacterial adhesion on antifouling polymer brushes via single-cell force spectroscopy, Polym. Chem. 6 (2015) 5740–5751, https://doi.org/10.1039/C5PY00197H.
[17] G. Cheng, G. Li, H. Xue, S. Chen, J.D. Bryers, S. Jiang, Zwitterionic carboxybetaine polymer surfaces and their resistance to long-term biofilm formation, Biomaterials 30 (2009) 5234–5240, https://doi.org/10.1016/j.biomaterials.2009.05.058.

[18] I. Francolini, C. Vuotto, A. Piozzi, G. Donelli, Antifouling and antimicrobial biomaterials: an overview, APMIS 125 (2017) 392–417, https://doi.org/10.1111/apm.12675.
[19] G.F. Rego, M.L. Vidal, G.M. Viana, L.M. Cabral, L.F.J. Schneider, M.B. Portela, L.M. Cavalcante, Antibiofilm properties of model composites containing quaternary ammonium methacrylates after surface texture modification, Dent. Mater. 33 (2017) 1149–1156, https://doi.org/10.1016/j.dental.2017.07.010.
[20] S. Chen, L. Liu, S. Jiang, Strong resistance of Oligo(phosphorylcholine) self-assembled monolayers to protein adsorption, Langmuir 22 (2006) 2418–2421, https://doi.org/10.1021/la052851w.
[21] A. Hasan, S.K. Pattanayek, L.M. Pandey, Effect of functional groups of self-assembled monolayers on protein adsorption and initial cell adhesion, ACS Biomater. Sci. Eng. 4 (2018) 3224–3233, https://doi.org/10.1021/acsbiomaterials.8b00795.
[22] N. Faucheux, R. Schweiss, K. Lutzow, C. Werner, T. Groth, Self-assembled monolayers with different terminating groups as model substrates for cell adhesion studies, Biomaterials 25 (2004) 2721–2730, https://doi.org/10.1016/j.biomaterials.2003.09.069.
[23] A. Roosjen, H.C. van der Mei, H.J. Busscher, W. Norde, Microbial adhesion to poly(ethylene oxide) brushes: influence of polymer chain length and temperature, Langmuir 20 (2004) 10949–10955, https://doi.org/10.1021/la048469l.
[24] S. Chen, L. Li, C. Zhao, J. Zheng, Surface hydration: principles and applications toward low-fouling/nonfouling biomaterials, Polymer 51 (2010) 5283–5293, https://doi.org/10.1016/j.polymer.2010.08.022.
[25] X. Zhang, L. Wang, E. Levänen, Superhydrophobic surfaces for the reduction of bacterial adhesion, RSC Adv. 3 (2013), https://doi.org/10.1039/c3ra40497h.
[26] H. Zhu, Z. Guo, W. Liu, Adhesion behaviors on superhydrophobic surfaces, Chem. Commun. (Camb.) 50 (2014) 3900–3913, https://doi.org/10.1039/c3cc47818a.
[27] D. Wang, Q. Sun, M.J. Hokkanen, C. Zhang, F.Y. Lin, Q. Liu, S.P. Zhu, T. Zhou, Q. Chang, B. He, Q. Zhou, L. Chen, Z. Wang, R.H.A. Ras, X. Deng, Design of robust superhydrophobic surfaces, Nature 582 (2020) 55–59, https://doi.org/10.1038/s41586-020-2331-8.
[28] C. Rodriguez Emmenegger, E. Brynda, T. Riedel, Z. Sedlakova, M. Houska, A.B. Alles, Interaction of blood plasma with antifouling surfaces, Langmuir 25 (2009) 6328–6333, https://doi.org/10.1021/la900083s.
[29] C. Rodriguez-Emmenegger, M. Houska, A.B. Alles, E. Brynda, Surfaces resistant to fouling from biological fluids: towards bioactive surfaces for real applications, Macromol. Biosci. 12 (2012) 1413–1422, https://doi.org/10.1002/mabi.201200171.
[30] E. Roeven, A.R. Kuzmyn, L. Scheres, J. Baggerman, M.M.J. Smulders, H. Zuilhof, PLL-poly(HPMA) bottlebrush-based antifouling coatings: three grafting routes, Langmuir 36 (2020) 10187–10199, https://doi.org/10.1021/acs.langmuir.0c01675.
[31] A.R. Kuzmyn, A.T. Nguyen, L.W. Teunissen, H. Zuilhof, J. Baggerman, Antifouling polymer brushes via oxygen-tolerant surface-initiated PET-RAFT, Langmuir 36 (2020) 4439–4446, https://doi.org/10.1021/acs.langmuir.9b03536.
[32] N.-P. Huang, R. Michel, J. Voros, M. Textor, R. Hofer, A. Rossi, D.L. Elbert, J.A. Hubbell, N.D. Spencer, Poly(l-lysine)-g-poly(ethylene glycol) layers on metal oxide surfaces: surface-analytical characterization and resistance to serum and fibrinogen adsorption, Langmuir 17 (2001) 489–498, https://doi.org/10.1021/la000736+.
[33] S. Tosatti, S.M. De Paul, A. Askendal, S. VandeVondele, J.A. Hubbell, P. Tengvall, M. Textor, Peptide functionalized poly(L-lysine)-g-poly(ethylene glycol) on titanium: resistance to protein adsorption in full heparinized human blood plasma, Biomaterials 24 (2003) 4949–4958, https://doi.org/10.1016/s0142-9612(03)00420-4.
[34] C. Rodriguez-Emmenegger, E. Brynda, T. Riedel, M. Houska, V. Subr, A.B. Alles, E. Hasan, J.E. Gautrot, W.T. Huck, Polymer brushes showing non-fouling in blood plasma challenge the currently accepted design of protein resistant surfaces, Macromol. Rapid Commun. 32 (2011) 952–957, https://doi.org/10.1002/marc.201100189.
[35] C. Rodriguez-Emmenegger, E. Brynda, T. Riedel, M. Houska, V. Šubr, A.B. Alles, E. Hasan, J.E. Gautrot, W.T.S. Huck, Polymer brushes showing non-fouling in blood plasma challenge the currently accepted design of protein resistant surfaces, Macromol. Rapid Commun. 32 (2011) 952–957, https://doi.org/10.1002/marc.201100189.
[36] J. Wei, D.B. Ravn, L. Gram, P. Kingshott, Stainless steel modified with poly (ethylene glycol) can prevent protein adsorption but not bacterial adhesion, Colloids Surf. B: Biointerfaces 32 (2003) 275–291, https://doi.org/10.1016/s0927-7765(03)00180-2.
[37] M. Rai, A. Yadav, A. Gade, Silver nanoparticles as a new generation of antimicrobials, Biotechnol. Adv. 27 (2009) 76–83, https://doi.org/10.1016/j.biotechadv.2008.09.002.
[38] S. Tang, J. Zheng, Antibacterial activity of silver nanoparticles: structural effects, Adv. Healthc. Mater. 7 (2018) e1701503, https://doi.org/10.1002/adhm.201701503.
[39] S. Vogt, K.D. Kühn, U. Gopp, M. Schnabelrauch, Resorbable antibiotic coatings for bone substitutes and implantable devices, Mater. Werkst. 36 (2005) 814–819, https://doi.org/10.1002/mawe.200500963.
[40] V. Albright, I. Zhuk, Y. Wang, V. Selin, B. van de Belt-Gritter, H.J. Busscher, H.C. van der Mei, S.A. Sukhishvili, Self-defensive antibiotic-loaded layer-by-layer coatings: imaging of localized bacterial acidification and pH-triggering of antibiotic release, Acta Biomater. 61 (2017) 66–74, https://doi.org/10.1016/j.actbio.2017.08.012.
[41] D. Pranantyo, L.Q. Xu, E.T. Kang, M.B. Chan-Park, Chitosan-based peptidopolysaccharides as cationic antimicrobial agents and antibacterial coatings, Biomacromolecules 19 (2018) 2156–2165, https://doi.org/10.1021/acs.biomac.8b00270.
[42] A. Rai, S. Pinto, M.B. Evangelista, H. Gil, S. Kallip, M.G. Ferreira, L. Ferreira, High-density antimicrobial peptide coating with broad activity and low cytotoxicity against human cells, Acta Biomater. 33 (2016) 64–77, https://doi.org/10.1016/j.actbio.2016.01.035.
[43] K. Yu, J.C. Lo, M. Yan, X. Yang, D.E. Brooks, R.E. Hancock, D. Lange, J.N. Kizhakkedathu, Anti-adhesive antimicrobial peptide coating prevents catheter associated infection in a mouse urinary infection model, Biomaterials 116 (2017) 69–81, https://doi.org/10.1016/j.biomaterials.2016.11.047.
[44] J.J. Oosterhof, K.J. Buijssen, H.J. Busscher, B.F. van der Laan, H.C. van der Mei, Effects of quaternary ammonium silane coatings on mixed fungal and bacterial biofilms on tracheoesophageal shunt prostheses, Appl. Environ. Microbiol. 72 (2006) 3673–3677, https://doi.org/10.1128/AEM.72.5.3673-3677.2006.
[45] B. Gottenbos, D.W. Grijpma, H.C.V.D. Mei, J. Feijen, H.J. Busscher, Antimicrobial effects of positively charged surfaces on adhering Gram-positive and Gram-negative bacteria, J. Antimicrob. Chemother. 48 (2001) 7–13, https://doi.org/10.1093/jac/48.1.7.
[46] J.M.R. Moreira, L.C. Gomes, K.A. Whitehead, S. Lynch, L.A. Tetlow, F.J. Mergulhão, Effect of surface conditioning with cellular extracts on *Escherichia coli* adhesion and initial biofilm formation, Food Bioprod. Process. 104 (2017) 1–12, https://doi.org/10.1016/j.fbp.2017.03.008.
[47] D. Cox, S.W. Kerrigan, S.P. Watson, Platelets and the innate immune system: mechanisms of bacterial-induced platelet activation, J. Thromb. Haemost. 9 (2011) 1097–1107, https://doi.org/10.1111/j.1538-7836.2011.04264.x.
[48] Z. Ferdous, A. Nemmar, Health impact of silver nanoparticles: a review of the biodistribution and toxicity following various routes of exposure, Int. J. Mol. Sci. 21 (2020), https://doi.org/10.3390/ijms21072375.
[49] E.M. Sussman, B.J. Casey, D. Dutta, B.J. Dair, Different cytotoxicity responses to antimicrobial nanosilver coatings when comparing extract-based and direct-contact assays, J. Appl. Toxicol. 35 (2015) 631–639, https://doi.org/10.1002/jat.3104.
[50] F. Pietsch, A.J. O'Neill, A. Ivask, H. Jenssen, J. Inkinen, A. Kahru, M. Ahonen, F. Schreiber, Selection of resistance by antimicrobial coatings in the healthcare setting, J. Hosp. Infect. 106 (2020) 115–125, https://doi.org/10.1016/j.jhin.2020.06.006.
[51] G. Xu, P. Liu, D. Pranantyo, L. Xu, K.-G. Neoh, E.-T. Kang, Antifouling and antimicrobial coatings from Zwitterionic and cationic binary polymer brushes assembled via "click" reactions, Ind. Eng. Chem. Res. 56 (2017) 14479–14488, https://doi.org/10.1021/acs.iecr.7b03132.
[52] K. Glinel, A.M. Jonas, T. Jouenne, J. Leprince, L. Galas, W.T. Huck, Antibacterial and antifouling polymer brushes incorporating antimicrobial peptide, Bioconjug. Chem. 20 (2009) 71–77, https://doi.org/10.1021/bc800280u.
[53] M. Kurowska, A. Eickenscheidt, D.L. Guevara-Solarte, V.T. Widyaya, F. Marx, A. Al-Ahmad, K. Lienkamp, A simultaneously antimicrobial, protein-repellent, and cell-compatible Polyzwitterion network, Biomacromolecules 18 (2017) 1373–1386, https://doi.org/10.1021/acs.biomac.7b00100.
[54] W.J. Yang, T. Cai, K.G. Neoh, E.T. Kang, G.H. Dickinson, S.L. Teo, D. Rittschof, Biomimetic anchors for antifouling and antibacterial polymer brushes on stainless steel, Langmuir 27 (2011) 7065–7076, https://doi.org/10.1021/la200620s.
[55] H. Vaisocherova, V. Sevcu, P. Adam, B. Spackova, K. Hegnerova, A. de los Santos Pereira, C. Rodriguez-Emmenegger, T. Riedel, M. Houska, E. Brynda, J. Homola, Functionalized ultra-low fouling carboxy- and hydroxy-functional surface platforms: functionalization capacity, biorecognition capability and resistance to fouling from undiluted biological media, Biosens. Bioelectron. 51 (2014) 150–157, https://doi.org/10.1016/j.bios.2013.07.015.
[56] U. Bog, A. de los Santos Pereira, S.L. Mueller, S. Havenridge, V. Parrillo, M. Bruns, A.E. Holmes, C. Rodriguez-Emmenegger, H. Fuchs, M. Hirtz, Clickable antifouling polymer brushes for polymer pen lithography, ACS Appl. Mater. Interfaces 9 (2017) 12109–12117, https://doi.org/10.1021/acsami.7b01184.
[57] V. Parrillo, A. de los Santos Pereira, T. Riedel, C. Rodriguez-Emmenegger, Catalyst-free "click" functionalization of polymer brushes preserves antifouling properties enabling detection in blood plasma, Anal. Chim. Acta 971 (2017) 78–87, https://doi.org/10.1016/j.aca.2017.03.007.
[58] J. Striebel, M. Vorobii, R. Kumar, H.-Y. Liu, B. Yang, C. Weishaupt, C. Rodriguez-Emmenegger, H. Fuchs, M. Hirtz, K. Riehemann, Controlled surface adhesion of macrophages via patterned antifouling polymer brushes, Adv. Biomed. Res. 1 (2020), https://doi.org/10.1002/anbr.202000029.
[59] A. de los Santos Pereira, T. Riedel, E. Brynda, C. Rodriguez-Emmenegger, Hierarchical antifouling brushes for biosensing applications, Sensors Actuators B Chem. 202 (2014) 1313–1321, https://doi.org/10.1016/j.snb.2014.06.075.
[60] C.R. Becer, R. Hoogenboom, U.S. Schubert, Click chemistry beyond metal-catalyzed cycloaddition, Angew. Chem. Int. Ed. Eng. 48 (2009) 4900–4908, https://doi.org/10.1002/anie.200900755.
[61] T. Gutsmann, I. Razquin-Olazaran, I. Kowalski, Y. Kaconis, J. Howe, R. Bartels, M. Hornef, T. Schurholz, M. Rossle, S. Sanchez-Gomez, I. Moriyon, G. Martinez de Tejada, K. Brandenburg, New antiseptic peptides to protect against endotoxin-mediated shock, Antimicrob. Agents Chemother. 54 (2010) 3817–3824, https://doi.org/10.1128/AAC.00534-10.
[62] L. Heinbockel, S. Sánchez-Gómez, G. Martinez de Tejada, S. Dömming, J. Brandenburg, Y. Kaconis, M. Hornef, A. Dupont, S. Marwitz, T. Goldmann, M. Ernst, T. Gutsmann, T. Schürholz, K. Brandenburg, Preclinical investigations reveal the broad-spectrum neutralizing activity of peptide Pep19-2.5 on bacterial pathogenicity factors, Antimicrob. Agents Chemother. 57 (2013) 1480–1487, https://doi.org/10.1128/aac.02066-12.
[63] L. Subh, W. Correa, T.-J. Pinkvos, P. Behrens, K. Brandenburg, T. Gutsmann, M.

Stiesch, K. Doll, A. Winkel, Synthetic anti-endotoxin peptides interfere with Gram-positive and Gram-negative bacteria, their adhesion and biofilm formation on titanium, J. Appl. Microbiol. 129 (2020) 1272–1286, https://doi.org/10.1111/jam.14701.

[64] S. Barcena-Varela, G. Martinez-de-Tejada, L. Martin, T. Schuerholz, A.G. Gil-Royo, S. Fukuoka, T. Goldmann, D. Droemann, W. Correa, T. Gutsmann, K. Brandenburg, L. Heinbockel, Coupling killing to neutralization: combined therapy with ceftriaxone/Pep19-2.5 counteracts sepsis in rabbits, Exp. Mol. Med. 49 (2017) e345, https://doi.org/10.1038/emm.2017.75.

[65] L. Martin, C. Peters, L. Heinbockel, J. Moellmann, A. Martincuks, K. Brandenburg, M. Lehrke, G. Müller-Newen, G. Marx, T. Schuerholz, The synthetic antimicrobial peptide 19-2.5 attenuates mitochondrial dysfunction in cardiomyocytes stimulated with human sepsis serum, Innate Immunity 22 (2016) 612–619, https://doi.org/10.1177/1753425916667474.

[66] L. Martin, K. Horst, F. Chiazza, S. Oggero, M. Collino, K. Brandenburg, F. Hildebrand, G. Marx, C. Thiemermann, T. Schuerholz, The synthetic antimicrobial peptide 19-2.5 attenuates septic cardiomyopathy and prevents down-regulation of SERCA2 in polymicrobial sepsis, Sci. Rep. 6 (2016) 37277, https://doi.org/10.1038/srep37277.

[67] J. Kohler, J. Ehler, B. Kreikemeyer, R. Bajorath, T. Schurholz, S. Oehmcke-Hecht, The synthetic LPS binding peptide 19-2.5 interferes with clotting and prevents degradation of high molecular weight kininogen in plasma, Sci. Rep. 10 (2020) 7142, https://doi.org/10.1038/s41598-020-64155-5.

[68] N. Sandetskaya, B. Engelmann, K. Brandenburg, D. Kuhlmeier, Application of immobilized synthetic anti-lipopolysaccharide peptides for the isolation and detection of bacteria, Eur. J. Clin. Microbiol. Infect. Dis. 34 (2015) 1639–1645, https://doi.org/10.1007/s10096-015-2399-5.

[69] K. Matyjaszewski, P.J. Miller, N. Shukla, B. Immaraporn, A. Gelman, B.B. Luokala, T.M. Siclovan, G. Kickelbick, T. Vallant, H. Hoffmann, T. Pakula, Polymers at interfaces: using atom transfer radical polymerization in the controlled growth of homopolymers and block copolymers from silicon surfaces in the absence of untethered sacrificial initiator, Macromolecules 32 (1999) 8716–8724, https://doi.org/10.1021/ma991146p.

[70] M.D. Jones, A.A. Brown, T.S.W. Huck, Surface-initiated polymerizations in aqueous media: effect of initiator density, Langmuir 18 (2002) 1265–1269, https://doi.org/10.1021/la011365f.

[71] J.M.R. Moreira, L.C. Gomes, J.D.P. Araújo, J.M. Miranda, M. Simões, L.F. Melo, F.J. Mergulhão, The effect of glucose concentration and shaking conditions on Escherichia coli biofilm formation in microtiter plates, Chem. Eng. Sci. 94 (2013) 192–199, https://doi.org/10.1016/j.ces.2013.02.045.

[72] L.C. Gomes, L.N. Silva, M. Simoes, L.F. Melo, F.J. Mergulhao, Escherichia coli adhesion, biofilm development and antibiotic susceptibility on biomedical materials, J. Biomed. Mater. Res. A 103 (2015) 1414–1423, https://doi.org/10.1002/jbm.a.35277.

[73] A. Heydorn, A.T. Nielsen, M. Hentzer, C. Sternberg, M. Givskov, B.K. Ersboll, S. Molin, Quantification of biofilm structures by the novel computer program COMSTAT, Microbiology (Reading, Engl.) 146 (Pt 10) (2000) 2395–2407, https://doi.org/10.1099/00221287-146-10-2395.

[74] S.V. Rao, K.W. Anderson, L.G. Bachas, Oriented immobilization of proteins, Mikrochim. Acta 128 (1998) 127–143, https://doi.org/10.1007/bf01243043.

[75] J.N. Walker, A.L. Flores-Mireles, C.L. Pinkner, H.L.t. Schreiber, M.S. Joens, A.M. Park, A.M. Potretzke, T.M. Bauman, J.S. Pinkner, J.A.J. Fitzpatrick, A. Desai, M.G. Caparon, S.J. Hultgren, Catheterization alters bladder ecology to potentiate *Staphylococcus aureus* infection of the urinary tract, Proc. Natl. Acad. Sci. U. S. A. 114 (2017) E8721–E8730, https://doi.org/10.1073/pnas.1707572114.

[76] J.M. Patti, M. Höök, Microbial adhesins recognizing extracellular matrix macromolecules, Curr. Opin. Cell Biol. 6 (1994) 752–758, https://doi.org/10.1016/0955-0674(94)90104-x.

[77] S.I. Faria, L.C. Gomes, R. Teixeira-Santos, J. Morais, V. Vasconcelos, F.J.M. Mergulhão, Developing new marine antifouling surfaces: learning from single-strain laboratory tests, Coatings 11 (2021), https://doi.org/10.3390/coatings11010090.

[78] L.C. Gomes, J. Deschamps, R. Briandet, F.J. Mergulhao, Impact of modified diamond-like carbon coatings on the spatial organization and disinfection of mixed-biofilms composed of *Escherichia coli* and *Pantoea agglomerans* industrial isolates, Int. J. Food Microbiol. 277 (2018) 74–82, https://doi.org/10.1016/j.ijfoodmicro.2018.04.017.

[79] T.R. Neu, J.R. Lawrence, [10] Lectin-binding analysis in biofilm systems, in: Methods Enzymol, Academic Press, 1999, pp. 145–152, https://doi.org/10.1016/S0076-6879(99)10012-0.

[80] A. Bridier, F. Dubois-Brissonnet, A. Boubetra, V. Thomas, R. Briandet, The biofilm architecture of sixty opportunistic pathogens deciphered using a high throughput CLSM method, J. Microbiol. Methods 82 (2010) 64–70, https://doi.org/10.1016/j.mimet.2010.04.006.

[81] E.A. Oniciuc, N. Cerca, A.I. Nicolau, Compositional analysis of biofilms formed by *Staphylococcus aureus* isolated from food sources, Front. Microbiol. 7 (2016) 390, https://doi.org/10.3389/fmicb.2016.00390.

[82] P. Alves, L.C. Gomes, C. Rodriguez-Emmenegger, F.J. Mergulhao, Efficacy of a poly(MeOEGMA) brush on the prevention of Escherichia coli biofilm formation and susceptibility, Antibiotics (Basel) 9 (2020), https://doi.org/10.3390/antibiotics9050216.

[83] L. Heinbockel, G. Weindl, W. Correa, J. Brandenburg, N. Reiling, K.H. Wiesmuller, T. Schurholz, T. Gutsmann, G. Martinez de Tejada, K. Mauss, K. Brandenburg, Anti-infective and anti-inflammatory mode of action of peptide 19-2.5, Int. J. Mol. Sci. 22 (2021), https://doi.org/10.3390/ijms22031465.

[84] W. Correa, J. Brandenburg, J. Behrends, L. Heinbockel, N. Reiling, L. Paulowski, D. Schwudke, K. Stephan, G. Martinez-de-Tejada, K. Brandenburg, T. Gutsmann, Inactivation of Bacteria by gamma-irradiation to investigate the interaction with antimicrobial peptides, Biophys. J. 117 (2019) 1805–1819, https://doi.org/10.1016/j.bpj.2019.10.012.

[85] H. Liao, L. Jiang, R. Zhang, Induction of a viable but non-culturable state in *Salmonella* Typhimurium by thermosonication and factors affecting resuscitation, FEMS Microbiol. Lett. 365 (2018), https://doi.org/10.1093/femsle/fnx249.